Seamless Switching Method Between Grid-Following and Grid-Forming Control for Renewable Energy Conversion Systems

Gao, Xian; Zhou, Dao; Anvari-Moghaddam, Amjad; Blaabjerg, Frede

Published in:
I E E E Transactions on Industry Applications

DOI (link to publication from Publisher):
10.1109/TIA.2024.3471728

Publication date:
2025

Document Version
Accepted author manuscript, peer reviewed version

Seamless Switching Method Between Grid-Following and Grid-Forming Control for Renewable Energy Conversion Systems

Xian Gao, *Member, IEEE,* Dao Zhou, *Senior Member, IEEE,* Amjad Anvari-Moghaddam, *Senior Member, IEEE,* and Frede Blaabjerg, *Fellow, IEEE*

***Abstract*— In alignment with decarbonization efforts, there has been widespread global interest in renewable energy sources such as wind and solar, which are connected to the grid via grid-connected inverters. The transition from traditional synchronous generator-based power systems to power-electronic-based power systems has introduced increased complexity due to the stochastic and intermittent nature of renewable energy outputs. Consequently, grid-connected inverters need to dynamically adapt their control strategies to cope with varying external grid conditions and ensure high reliability. However, such transitions can cause abrupt changes in the control loops (e.g., power loop or voltage loop), and lead to voltage and current distortions, potentially compromising safe operation. To address this issue, this paper proposes a smooth switching method between the grid-following (GFL) and grid-forming (GFM) control in grid-connected mode. This method can improve the control flexibility of the grid-connected converters and broaden the stability boundary of the power system. The proposed method is verified in a case study of a 15.8 kVA grid-connected converter. Time-domain simulations carried out in Matlab/Simulink and an established experimental prototype are applied to verify the effectiveness of the proposed control method. The results demonstrate that the proposed control method effectively mitigates voltage and current distortions during transitions, ensuring safer and more reliable operation.**

***Index Terms*—Renewable energy sources, grid-connected inverters, seamless switching method, grid-following (GFL) control, grid-forming (GFM) control.**

I. Introduction

With the intensification of the global energy crisis and environmental problems, renewable energy sources have been developed vigorously [1], [2]. The integration of distributed energy into power grids is increasing year by year. The distributed energy is usually connected to the power grid through power electronic inverters. They have two common control modes of the inverter [3]. One is the grid-following (GFL) control, regulating the active and reactive power injected into the power grid with a fast response but providing almost no moment of inertia for the system, and utilizing a phase-locked loop (PLL) for synchronization, which cannot operate in a stand-alone mode [4]. The other one is the grid-forming (GFM) control, regulating the frequency and voltages of the inverter and providing inertia and damping for the power system, which enables it to operate both in the grid-tied mode and the stand-alone mode [5].

Based on the prior art studies [6], it has been revealed that the GFL converter suffers from instability in power grids with low short-circuit ratios (SCR), while the GFM converter suffers from instability in power grids with high SCR [7], [8]. It indicates that the GFL converter can be more suitable for the stiff power grid while the GFM converter is more suitable for the weak power grid. Considering the different performances of the GFL and GFM converters operation in the power grids with various SCRs, some coordination technologies are proposed. A secondary control scheme that coordinates the GFL and GFM converters for restoring frequency and voltage in a microgrid with 100% inverter-based generation is proposed in [9]. It adopts a leader-follower consensus framework, with GFL inverters acting as followers and GFM inverters acting as leaders. In [10], an optimal placement strategy of the GFM converters is proposed to enhance the small-signal stability of PLL-integrated power grids. However, they just consider the placement and power sharing among the GFL and GFM converters, neglecting the seamless transitions between them, which lack the control flexibility.

In order to make full use of the GFL and GFM converters, numerous methods have been proposed for the three-phase inverters to realize a smooth transition between the GFL and GFM control [11]-[24]. In [13], two semi-parallel control paths are proposed for the GFL and GFM modes respectively. The two control paths remain synchronized throughout the operation of the inverter to realize smooth switching. It is worth noting that during the synchronization process, the inverters remain connected to the system without any power injection, named standby mode. Following the completion of synchronization in standby mode, the inverter can change to its desired mode of operation. Authors of [16] introduce a method for the seamless restoration of power to critical infrastructure. Under grid-tied mode, the inverters don't generate any active and reactive power, leaving the entire load to be supported by the grid, working in a standby mode. The primary objective is just to ensure the secure operation of critical infrastructures, with the GFM inverters functioning akin to a backup. A unified control method of the grid-connected inverters for a smooth transfer to stand-alone mode regardless of whether the system is exporting power to or importing power from the grid is

proposed in [18]. The proposed scheme is designed to avoid any modifications in the control loops and the need to impose initial values on the compensators during the mode transfer. In [20], a seamless switching control strategy based on model prediction is proposed to realize maximum power tracking under grid-tied mode and voltage regulation under islanded mode. An autonomous control strategy of inverters realizing smooth switching of sudden islanding and reconnection without the requirement of communication is proposed in [21] and [22]. In [23], a compensation loop is designed and added to the excitation loop to realize the seamless transition without any external signals from the detection scheme of the islanding. A multifunctional converter is proposed in [24], which can operate either as a voltage- or current-controlled source and realize a smooth transition between the two operating modes.

However, the majority of these research works focus on the transitions between the grid-tied mode and the stand-alone mode, where the GFL control is applied in the grid-tied mode, while the GFM control is applied in the stand-alone mode. Moreover, they do not allow any power exchange between the converters and the power grids during the transition. Thus, there is still a scarcity of papers addressing transitions specifically between the GFL and GFM converters within the grid-tied mode, which can improve the control flexibility of the grid-connected converters. In addition, during the transition, the inverters still can be allowed to inject non-zero power into the power grid.

Notably, a weak power grid poses challenges to the PLL synchronization and will also adversely affect the stable operation of GFL inverters [25], [26]. The GFL inverters possess a weaker power transfer ability under a weak power grid [27]. Instability problems may occur when the generation capacity from renewable energy sources is substantial, such as in scenarios involving intense irradiance in photovoltaic systems with high-power ratings. Thus, under this scenario, the GFM control is preferred, and the GFL control needs to change to the GFM control to ensure the stable operation. Conversely, when connected to a strong power grid, the inverter and the grid essentially act as two voltage sources in parallel, separated by a relatively small impedance. In such cases, even a minor phase difference may induce significant active power fluctuations under the GFM control, potentially leading to an overload of the system [28], [29]. In this case, the GFL control is preferred and the GFM control needs to change to the GFL control.

Therefore, it is crucial to recognize that, for the distributed renewable energy generation system, it may be necessary to change the control mode of grid-connected inverters to maintain the stability of the power system under varying working conditions. During the grid-connected mode, transitions between the GFL and GFM control are indispensable for broadening the stability boundary of the power system. Furthermore, the seamless transitions in the situations in which the inverters inject non-zero power into the power grid also need to be considered.

To achieve optimal performance across diverse operational conditions and leverage the benefits of both the GFL control and GFM control, this paper aims to introduce a straightforward switching control strategy, facilitating seamless transitions between the GFL and GFM control. The main contributions can be summarized as follows. (1) Comprehensive illustrations of the mathematical models of a typical three-phase grid-connected system are given. (2) Each control loop of both the GFL and GFM control is discussed in detail. (3) A straightforward seamless switching method is presented to realize a smooth transition between the GFL and GFM control under the grid-connected mode no matter whether there is any power transfer between the converter and the power grid.

The rest of this paper is organized as follows. Section II gives the modeling of a three-phase grid-connected voltage source converter. In Section III, each control loop of both the GFL and GFM control is presented in detail, and the seamless switching method is proposed. In Section IV, a time-domain simulation model is built in MATLAB/Simulink to verify the effectiveness of the proposed seamless switching method. Section V provides an experimental validation. Finally, conclusions are drawn in Section VI.

II. Modeling of a Three-Phase Grid-Connected Voltage Source Converter

Three-phase power converters are widely used in renewable energy sources, e.g., wind and photovoltaic power generation. The topology of a grid-connected power converter system is shown in Fig. 1, where the system consists of a three-phase inverter, an LC filter, a grid impedance and a power grid. L_f and C_f are the inductor and the capacitor of the LC filter; Z_g is the equivalent grid impedance; u_{dc} is the dc-link voltage; u_a, u_b and u_c are the converter output voltages; u_{pcca}, u_{pccb} and u_{pccc} are the voltages at the point of common coupling (PCC); u_{ga}, u_{gb} and u_{gc} are the grid voltages; i_a, i_b and i_c are the converter output currents; i_{ga}, i_{gb} and i_{gc} are the grid currents; i_{Ca}, i_{Cb} and i_{Cc} are the capacitor currents.

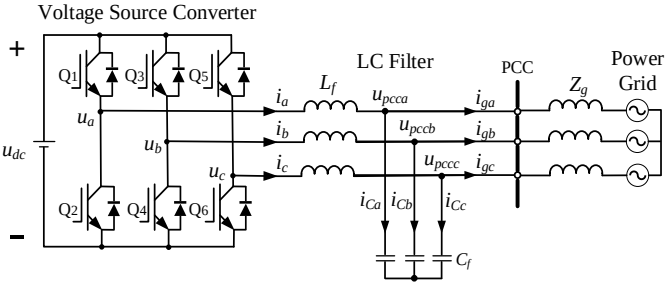

Fig. 1. Typical configuration of a grid-connected voltage source converter.

Defining δ as the power angle, which is the phase angle difference between the PCC voltage vector $U_{pcc}\angle\delta$ and the grid voltage vector $U_g\angle 0$. α represents the angle of the grid impedance. The phase relationship between the PCC and the power grid is shown in Fig. 2.

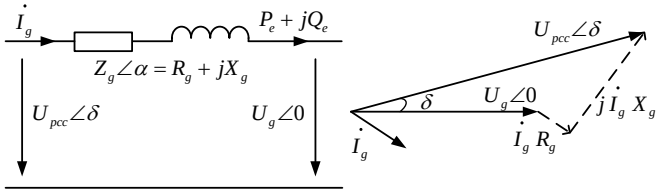

Fig. 2. Phase relationship between the PCC and power grid voltages.

The active power p and the reactive power q flowing from the PCC to the power grid can be given as:

$$\begin{cases} p = \left(3U_{pcc}{}^2 \cos\alpha - 3U_{pcc}U_g \cos(\alpha+\delta)\right)/Z_g \\ q = \left(3U_{pcc}{}^2 \sin\alpha - 3U_{pcc}U_g \sin(\alpha+\delta)\right)/Z_g \end{cases} \tag{1}$$

In this paper, the synchronizing frame is defined by ω, which is synchronized to the voltage phase angle at the PCC. According to Kirchhoff's voltage law, the mathematical model of the main circuit in the ω-defined rotating d-q frame can be achieved as [30], [31]:

$$u_{pccd} - u_g \cos\delta = L_g \frac{di_{gd}}{dt} + R_g i_{gd} - \omega L_g i_{gq} \tag{2}$$

$$u_{pccq} + u_g \sin\delta = L_g \frac{di_{gq}}{dt} + R_g i_{gq} + \omega L_g i_{gd} \tag{3}$$

$$i_d - i_{gd} = C_f \frac{du_{pccd}}{dt} - \omega C_f u_{pccq} \tag{4}$$

$$i_q - i_{gq} = C_f \frac{du_{pccq}}{dt} + \omega C_f u_{pccd} \tag{5}$$

$$u_d - u_{pccd} = L_f \frac{di_d}{dt} - \omega L_f i_q \tag{6}$$

$$u_q - u_{pccq} = L_f \frac{di_q}{dt} + \omega L_f i_d \tag{7}$$

where subscripts d and q represent the d-axis and q-axis components of a variable, respectively.

Under the d-q frame, the expression of the output active power and reactive power can be given as:

$$\begin{cases} p = 1.5\left(u_{pccd}i_{gd} + u_{pccq}i_{gq}\right) \\ q = 1.5\left(-u_{pccd}i_{gq} + u_{pccq}i_{gd}\right) \end{cases} \tag{8}$$

III. Smooth Switching Method

In this paper, the active and reactive power control (PQ control) and the virtual synchronous generator control (VSG control) are adopted as the GFL control and the GFM control, respectively. The proposed control schemes of the proposed smooth switching method are shown in Fig. 3.

The control system consists of a grid synchronization loop, a power loop, an excitation loop, a voltage loop and a current loop. The grid synchronization loop is composed of two parts: the phase-locked loop (PLL) for the GFL control and the power synchronization loop for the GFM control. The control system is performed under the control synchronizing frame (defined by the grid synchronization loop), while the electrical system is performed under the actual system synchronizing frame (defined by the PCC voltage) [32]. While the two synchronizing frames align during the steady-state operation, a minor difference arises during the dynamic state. To improve the model accuracy, this discrepancy is considered, and variables within the control synchronizing frame are denoted with a superscript c, while variables within the actual system synchronizing frame are denoted with a superscript s.

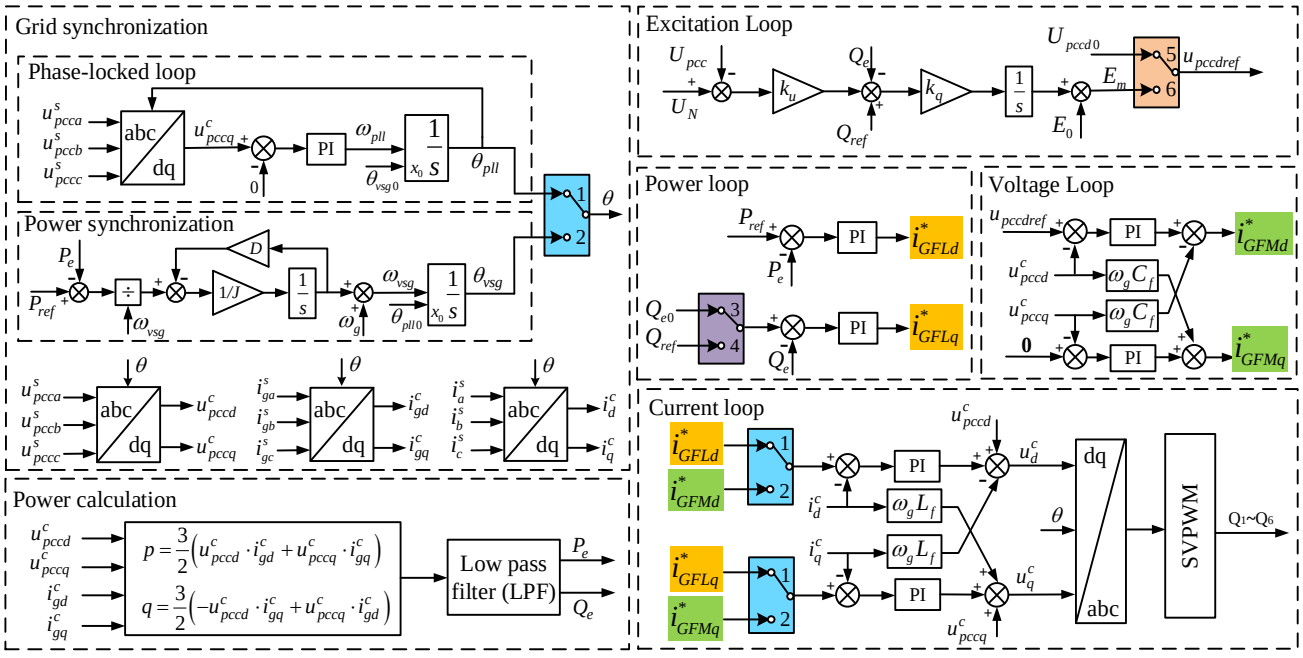

Fig. 3. Control schemes of the smooth switching method between grid-following and grid-forming control.

A. Grid-following control

The GFL control consists of the PLL unit, a power loop and a current loop. The GFL control adopts a PLL unit to enable the inverter synchronized to the power grid. The outer power control loop regulates the active and reactive power injected into the power grid. The outer power loop generates references for the current loop, denoted as i^*_{GFLd} and i^*_{GFLq}, respectively. The outputs of the power loop can be given as follows:

$$\begin{cases} i^*_{GFLd} = \left(k_{pPQ} + k_{iPQ}/s\right)\left(P_{ref} - P_e\right) \\ i^*_{GFMq} = -\left(k_{pPQ} + k_{iPQ}/s\right)\left(Q_{ref} - Q_e\right) \end{cases} \tag{9}$$

where k_{pPQ} and k_{iPQ} are the proportional and integral coefficients of the power controller.

To track the references set by the outer power loop, the inner current loop is adopted to adjust the converter currents. The outputs of the current loop can be given as follows:

$$\begin{cases} u^c_d = \left(k_{pc} + k_{ic}/s\right)\left(i^*_{GFLd} - i^c_d\right) - \omega_g L_f i^c_q + u^c_{pccd} \\ u^c_q = \left(k_{pc} + k_{ic}/s\right)\left(i^*_{GFMq} - i^c_q\right) + \omega_g L_f i^c_d + u^c_{pccq} \end{cases} \tag{10}$$

where k_{pc} and k_{ic} are the proportional and integral coefficients of the current controller; ω_g presents the grid angular frequency.

B. Grid-forming control

The GFM control is composed of a power synchronization loop, an excitation loop, a voltage loop and a current loop. Unlike the GFL control, the GFM control does not need a PLL unit for synchronization. Instead, it emulates the power synchronization characteristics of conventional synchronous generators, represented by the swing equation:

$$\begin{cases} J\dfrac{d\omega_{vsg}}{dt} = \dfrac{P_{ref}}{\omega_{vsg}} - \dfrac{P_e}{\omega_{vsg}} - D\left(\omega_{vsg} - \omega_g\right) \\ d\theta_{vsg}/dt = \omega_{vsg} \end{cases} \tag{11}$$

where J denotes the moment of inertia; D denotes the damping coefficient; ω_{VSG} denotes the angular frequency of the VSG control.

The excitation loop adopts the droop control using an integrator, which is also called droop-I control [33]. The excitation loop can be given as follows:

$$E_m = E_0 + k_q \int \left(k_u\left(U_N - u_{pcc}\right) + Q_{ref} - Q_e\right) \tag{12}$$

where k_q is an integral gain; k_u is the voltage droop coefficient; E_0 is the no-load electromotive force of the converter; U_N is the peak value of the rated grid voltage.

The voltage loop regulates the PCC voltages to track the references set by the excitation loop, which can be given as follows:

$$\begin{cases} i^c_{dref} = \left(k_{pu} + k_{iu}/s\right)\left(u_{pccdref} - u^c_{pccd}\right) - \omega_g C_f u^c_{pccq} \\ i^c_{qref} = \left(k_{pu} + k_{iu}/s\right)\left(0 - u^c_{pccq}\right) + \omega_g C_f u^c_{pccd} \end{cases} \tag{13}$$

where k_{pu} and k_{iu} are the proportional and integral coefficients of the voltage controller.

The current loop of the GFM control is almost the same as that of the GFL control. The only difference is that the references of the current loop under the GFM control are determined by the voltage control, while the references of the current loop under the GFL control are determined by the outer power control. Thus, it will not be described in details here. The references of the current loop under the GFM control are defined as i^*_{GFMd} and i^*_{GFMq}.

C. Smooth control switching method between the grid-forming and grid-following control

In the case that both the GFL and GFM control schemes have the same inner current loop, only the outer loops should be regulated during the switching period. To ensure this smooth transition, it is crucial to maintain consistent references for the inner current loop of both control modes. In addition, the steady-state operation points before and after the transition should remain unchanged [34]. The flow chart of the proposed seamless switching method is shown in Fig. 4. The switch signal is given by the extra controller, which depends on the external grid strength. In practical implementation, the renewable energy conversion system may constantly encounter changes in operational scenarios, characterized by fluctuations in renewable energy sources generation, which leads to time-varying system stability. Consequently, a consensus has been drawn by both the industry and academia that it is important to conduct real-time monitoring of system strength within renewable energy conversion systems [35]. A generalized SCR (gSCR) is proposed to assess the stability of multi-infeed power electronic systems [36]. Based on this, a distributed power method developed to calculate the gSCR in real time is proposed in [37], which can be an efficient tool to identify the strength of the external grid and determine the switch signal.

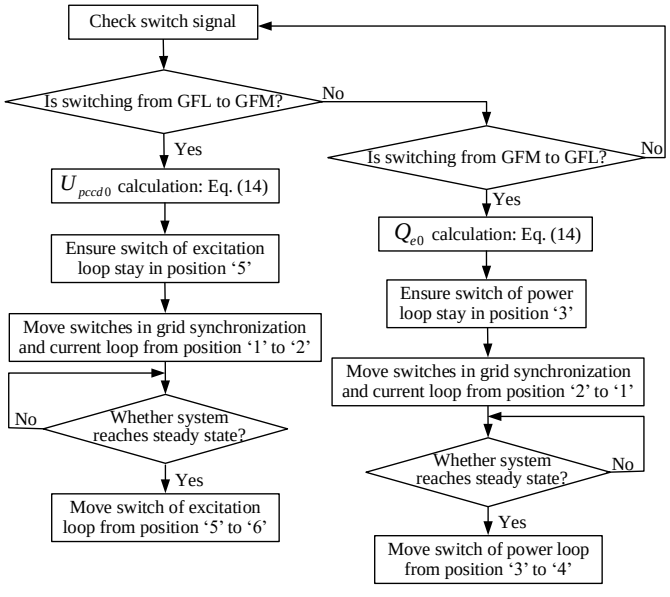

Fig. 4. Flow chart of the proposed seamless switching method.

Because the change occurs under the grid-connected mode, when the P_{ref} for both the GFL and GFM controls is set to the same value, the output of the power synchronization loop ω_{vsg} is the same as that of the PLL unit ω_{pll} during the steady-state. Thus, it is possible to realize the smooth switching in the grid synchronization part. During the transition from the GFM control to the GFL control, the grid synchronization part should

be changed from the power synchronization loop to the PLL unit. To achieve this, the output of the integrator in the power synchronization θ_{vsg0} should be set as the initial value of the integrator in the PLL unit during the transition, and the switch in the grid synchronization part is required to change from position '2' to '1'. Conversely, when switching from the GFL control to the GFM control, the grid synchronization part should be altered from the PLL unit to the power synchronization loop. The output of the integrator in the PLL unit θ_{pll0} should be set as the initial value of the integrator in the power synchronization during the transition, and the switch in the grid synchronization part is required to change from position '1' to '2'.

To ensure consistent steady-state operation points before and after the transition from the GFM control to the GFL control, P_{ref} and Q_{ref} of the GFL control should be set as the same values as P_{e0} and Q_{e0} of the GFM control under the steady-state operation. Because the converter is connected to the power grid, the frequency is equal to ω_g. Hence, P_{ref} and P_{e0} are the same. However, for the Q_e, due to the regulation of the excitation loop, there is a droop relationship between the reactive power and the voltages at the PCC during the steady-state operation, which can be expressed as:

$$k_u\left(U_N - U_{pcc}\right) + Q_{ref} - Q_e = 0 \tag{14}$$

It can be observed that when the PCC voltage deviates from the rated grid voltage U_N, the Q_e under the GFM control will not track the Q_{ref}, which may result in differences in the steady-state operation points before and after the transition. To address this issue, it is necessary to calculate and set the steady-state value Q_{e0} of the GFM control as Q_{ref} for the GFL control. By combining (1)-(8) and (14), the steady-state value of the output reactive power Q_{e0} can be calculated. During the transition from the GFM control to the GFL control, the switch in the power control loop should be in position '3' to ensure consistency in the operation point before and after the transition. The switch in the current control part is needed to switch from position '2' to '1'. Once the converter can effectively track P_{ref} and Q_{ref}, the switch in the power control loop can switch to position '4' to regulate the Q_e tracking the Q_{ref}.

Conversely, when changing from the GFL control to the GFM control, in order to ensure the same steady-state operation points before and after the transition, $u_{pccdref}$ and $u_{pccqref}$ of the GFM control should be set as the same values as U_{pccd0} and U_{pccq0} of the GFL control under steady-state operation. Notably, during the steady-state operation, the $u_{pccqref}$ and U_{pccq0} are both equal to 0, so only $u_{pccdref}$ and U_{pccd0} need to be considered. By combining (1)-(8) and assuming P_e and Q_e can well track the references P_{ref} and Q_{ref} without any steady state error, the U_{pccd0} can be calculated. During the transition from the GFL control to the GFM control, the switch in the current control part should switch from position '1' to '2' and the excitation loop is not activated where the switch should be in position '5'. After the switching, when the converter enters into steady-state operation, the excitation loop is enabled, and the switch should be in position '6'.

IV. Simulation Model and Results

In order to verify the effectiveness of the proposed smooth switching method, a case study system is established in MATLAB/Simulink [1]. The key parameters of the case study are listed in TABLE I [38]. Moreover, the proposed smooth switching method is applied in both the strong and weak power grids. The SCR is set as 10 and 1.5 for the study.

TABLE I
Parameters of a Grid-Connected Converter

Grid Parameters		
u_g	Grid phase voltage	311 V (1 p.u.)
f_g	Grid frequency	50 Hz (1 p.u.)
ω_g	Grid angular frequency	314 rad/s (1 p.u.)
SCR	Short-circuit ratio	10 (strong power grid)/ 1.5 (weak power grid)
L_g	Grid impedance	2.9/19.3 mH (0.1/0.66 p.u.)
R_g	Grid resistance	0.09/0.96 Ω (0.01/0.1 p.u.)
Converter Parameters		
u_{dc}	DC-side voltage	700 V
L_f	Filter inductance	4 mH (0.14 p.u.)
C_f	Filter capacitance	10 μF (0.03 p.u.)
S_n	Nominal power	15.8 kVA (1 p.u.)
f_s	Switching frequency	10 kHz
f_{sa}	Sampling frequency	10 kHz
Controller Parameters		
P_{ref}	Active power reference	0.5 p.u.
Q_{ref}	Reactive power reference	0 p.u.
E_0	No-load electromotive force of the converter	1 p.u.
U_N	Peak value of the rated grid voltage	1 p.u.
k_u	Q-U loop coefficient	3 p.u.
k_q	Integrity coefficient	0.02 p.u.
D	Damping coefficient	100 p.u.
J	Virtual inertia	1 p.u.
k_{pu}/k_{iu}	Voltage controller	0.3/100 p.u.
k_{ppll}/k_{ipll}	Phase-locked loop	0.13/2.3 p.u.
k_{pPQ}/k_{iPQ}	Power controller	0.1/60 p.u.
k_{pc}/k_{ic}	Current controller	2/200 p.u.
ω_c	Cut-off frequency of low-pass filter	20 Hz

When the converter changes from the GFM control to the GFL control, the steady-state value of the reactive power Q_{e0} under the GFM control needs to be calculated. The output reactive power of the GFM control has a droop relationship with the PCC voltage, as expressed in (14). Because of the regulation of the voltage control loop, the steady-state value of the q-axis component of the PCC voltage U_{pccq0} is 0, and the steady-state value of the PCC voltage U_{pcc0} is equal to its d-axis component U_{pccd0}. Based on the analysis above and the parameters shown in TABLE I, setting all the differential terms as 0 in (2)-(7) and combining (1), (8) and (14), the steady-state value of the reactive power Q_{e0} can be calculated. In the case of SCR is 10, the Q_{e0} is -1.3 Var, and in the case of SCR is 1.5,

the Q_{e0} is -6 Var.

Similarly, when the converter changes from the GFL control to the GFM control, the steady-state value of the d-axis component and the q-axis component of the PCC voltage U_{pccd0} and U_{pccq0} under the GFL control need to be calculated, respectively. In the case of the GFL converter, because of the regulation of the power control loop, the output active power P_e and reactive power Q_e are equal to P_{ref} and Q_{ref}. Furthermore, due to the presence of the PLL unit, U_{pccq0} is 0. By considering the parameters shown in TABLE I, setting all the differential terms as 0 in (2)-(7) and combining (1) and (8), the steady-state value of the d-axis component of the PCC voltage U_{pccd0} can be calculated. In the case of SCR is 10, the U_{pccd0} is 313 V., and in the case of SCR is 1.5, the U_{pccd0} is 310 V.

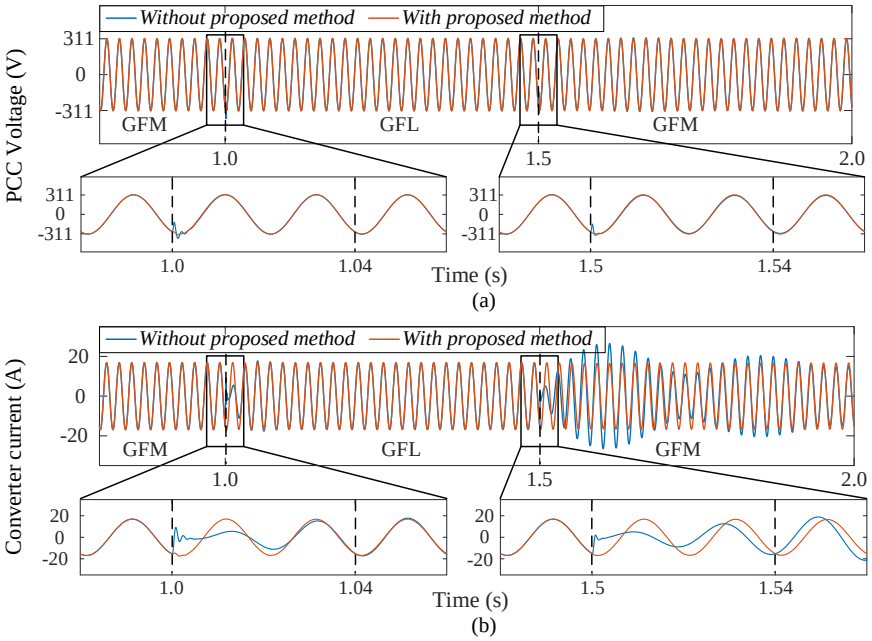

Fig. 5. Simulation results of switching between grid-forming and grid-following control without and with proposed smooth switching control. (a) PCC voltages; (b) Converter output currents (SCR=10).

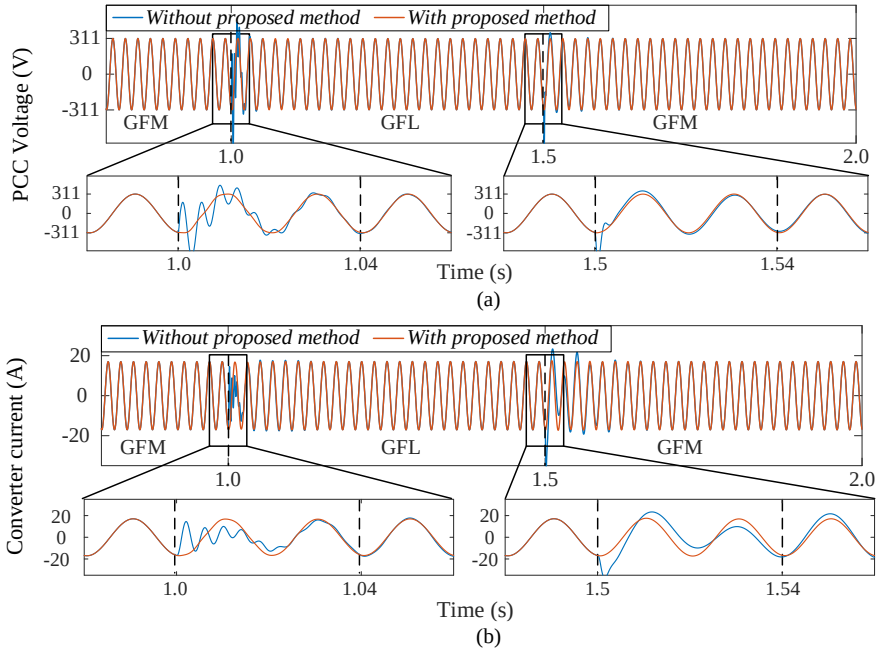

Fig. 6. Simulation results of switching between grid-forming and grid-following control without and with proposed smooth switching control. (a) PCC voltages; (b) Converter output currents (SCR=1.5).

When the power grid is strong and the SCR is 10, the simulation results of switching between the GFM and GFL control without and with the proposed smooth switching control are shown in Fig. 5. The control mode changes from the GFM to GFL control at t=1s and changes from the GFL to GFM control at t=1.5s. The reference of reactive power control changes from Q_{e0} to 0 at t=1.04s, and the excitation loop is activated at t=1.54s. Both the PCC voltage and converter

current have some oscillations during the switching period without the proposed smooth switching control. However, with the smooth switching control, during the switching time, the oscillations of both the PCC voltages and converter currents are effectively reduced. In addition, the total harmonic distortions (THD) are also reduced. The THD of the PCC voltage and converter current without and with the proposed seamless switching method is summarized in TABLE II.

Similarly, the same comparisons are also adopted in the weak power grid. When the SCR is 1.5, the simulation results of switching between the GFM and GFL control without and with the proposed smooth switching control are shown in Fig. 6. During the switching period, the PCC voltages and converter currents undergo oscillations without the smooth switching control. However, when the proposed method is adopted, both the PCC voltages and converter currents have realized a smooth switching.

TABLE II

THD OF VOLTAGE AND CURRENT WITH AND WITHOUT PROPOSED METHOD

Mode Transition \ Grid Strength		SCR=1.5		SCR=10	
		Voltage	Current	Voltage	Current
GFM ↓ GFL	Without proposed method	44.74%	50.01%	5.80%	39.77%
	With proposed method	1.98%	2.13%	0.64%	3.11%
GFL ↓ GFM	Without proposed method	19.35%	17.56%	3.96%	22.41%
	With proposed method	0.16%	0.22%	0.16%	1.59%

Therefore, through the simulation results, it is evident that the proposed straightforward strategy can realize seamless transitions between the GFL and GFM control regardless of whether the power grid is strong or weak.

V. EXPERIMENTAL VALIDATION

To validate the efficiency of the proposed seamless switching method, a three-phase grid-connected system setup is used as illustrated in Fig. 7. The parameters of the experimental setup are the same as those specified in TABLE I in Section IV. The three-phase grid-connected converter is based on the Imperix standard PEB-SiC-8024 module. The power grid is simulated by three high-fidelity linear amplifiers APS 15000. The converter currents and grid currents are measured by the LEM LAH50-P current sensors, while the PCC voltages are measured by the LEM LV20-P voltage sensors. All the measured data are transmitted to the B-BOX RCP control platform. The control algorithm is coded in a personal computer and loaded to the B-BOX RCP control platform via a patch cable. The real-time monitoring and the adjustment of control variables are carried out using the Imperix cockpit.

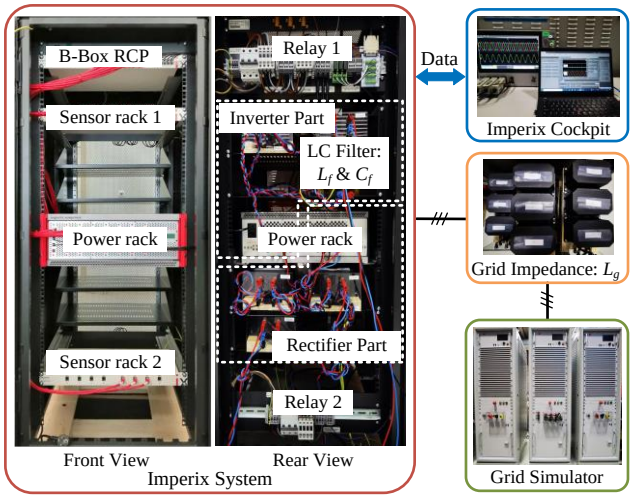

Fig. 7. Experimental setup of a three-phase grid-connected system.

When the power grid is weak and the SCR is 1.5, the experimental results are as shown in Fig. 8 - Fig. 11. During the transition from the GFM to GFL control, the experimental waveforms of the PCC voltages and converter currents without the smooth switching control are shown in Fig. 8. During the switching time, the converter outputs have large oscillation, which leads to a shutdown of the converter. When the smooth switching control is applied, the experimental waveforms of PCC voltages and converter currents are shown in Fig. 9. In this case, both the PCC voltages and converter currents have realized a smooth transition. It is worth mentioning that when the SCR is 1.5, the waveforms of the currents are distorted under the GFL control which indicates that the GFL converter is not suitable for a very weak power grid.

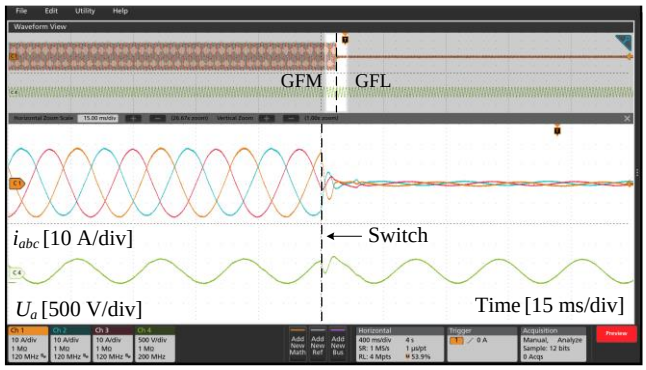

Fig. 8. Experimental waveforms of PCC voltages and converter currents changing from grid-forming to grid-following without smooth switching control (SCR=1.5).

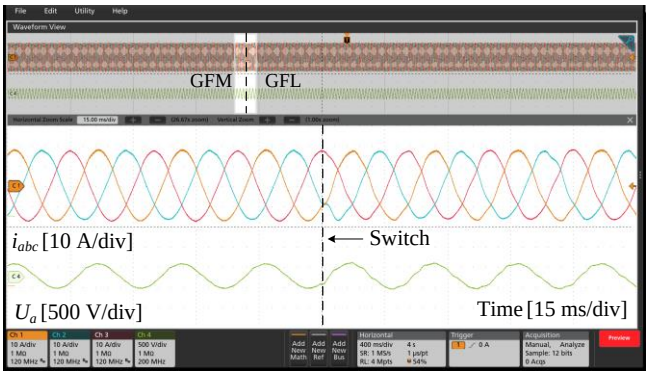

Fig. 9. Experimental waveforms of PCC voltages and converter currents changing from grid-forming to grid-following with smooth switching control (SCR=1.5).

During the transition from the GFL to GFM control, the experimental waveforms of PCC voltages and converter currents without a smooth switching control are shown in Fig.

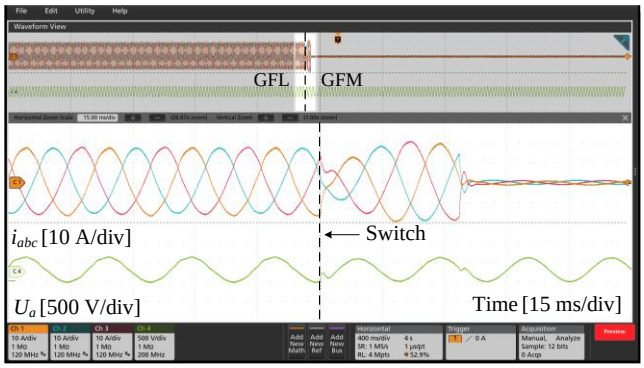

Fig. 10. Experimental waveforms of PCC voltages and converter currents changing from grid-following to grid-forming without smooth switching control (SCR=1.5).

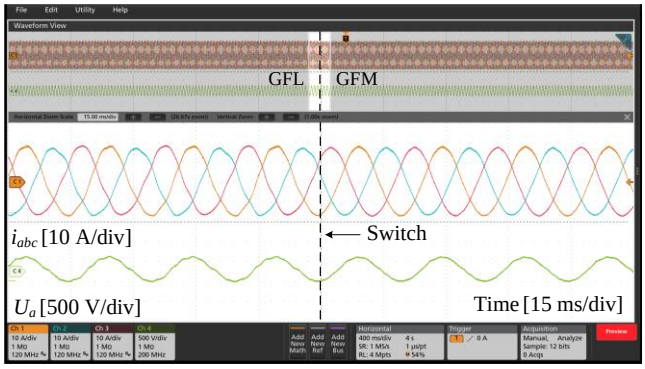

Fig. 11. Experimental waveforms of PCC voltages and converter currents changing from grid-following to grid-forming with smooth switching control (SCR=1.5).

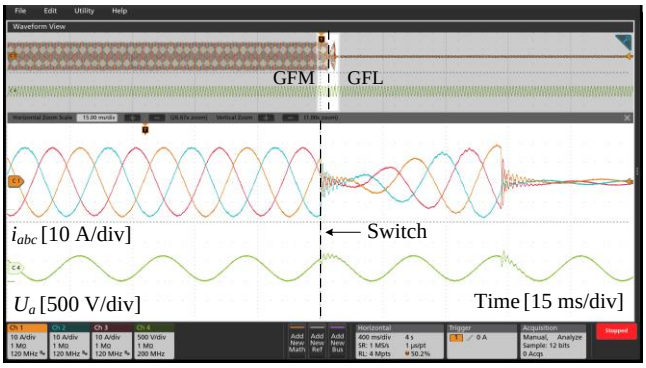

Fig. 12. Experimental waveforms of PCC voltages and converter currents changing from grid-forming to grid-following without smooth switching control (SCR=10).

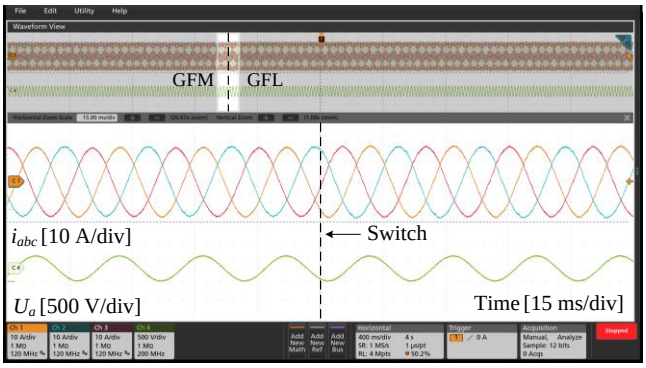

Fig. 13. Experimental waveforms of PCC voltages and converter currents changing from grid-forming to grid-following with smooth switching control (SCR=10).

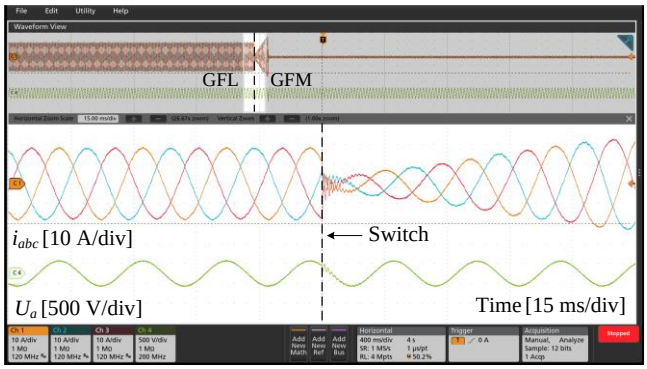

Fig. 14. Experimental waveforms of PCC voltages and converter currents changing from grid-following to grid-forming without smooth switching control (SCR=10).

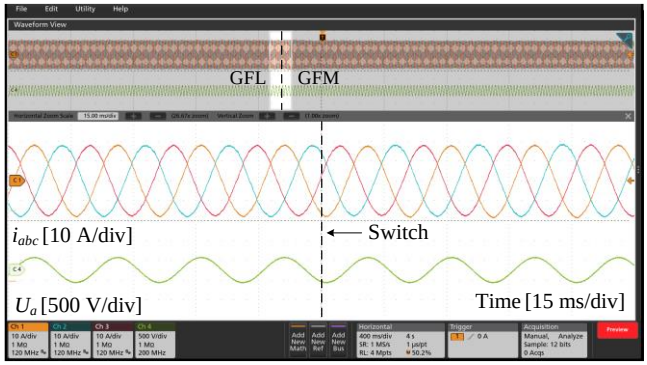

Fig. 15. Experimental waveforms of PCC voltages and converter currents changing from grid-following to grid-forming with smooth switching control (SCR=10).

10. The experimental waveforms of PCC voltages and converter currents with the smooth switching control are shown in Fig. 11. Without the proposed method, the large oscillations during the transition leads to the trigger of the hardware protection. With the proposed control, it is clear that the proposed smooth switching control works well and gives obviously a much smoother transition between the GFL control and GFM control.

Similarly, the same experiments are carried out in a strong power grid. When the SCR is 10, the experimental results are shown in Fig. 12 - Fig. 15. When the control mode changes from the GFM to GFL control, the experimental waveforms of the PCC voltages and converter currents without and with the smooth switching control are shown in Fig. 12 and Fig. 13. When the control mode changes from the GFL to GFM control, the experimental waveforms of the PCC voltages and converter currents without and with the smooth switching control are shown in Fig. 14 and Fig. 15. It is evident that the implementation of the proposed smooth switching control effectively ensures the safe operation, and a smooth transition between the GFL and GFM control.

VI. Conclusion

To cope with the complex working conditions introduced by the stochastic and intermittent nature of renewable energy sources, grid-connected inverters need to dynamically adapt their control strategies to cope with varying external grid

conditions. The GFL and GFM control are suitable for different levels of grid strength. Therefore, a collective control design can be implemented to optimize performance based on external grid conditions, thus achieving a unified control structure for grid-connected inverters. This paper proposes a straightforward smooth switching method to facilitate seamless transitions between the GFL and GFM control in the grid-connected mode. The key to achieving seamless switching is to maintain consistent operation points before and after the transition.

The proposed seamless switching method leverages the advantages of both the GFL and GFM converters, enhancing the control flexibility of grid-connected converters and broadening the stability boundaries of power grids. In addition, the method allows inverters to inject non-zero power into the grid during transitions, ensuring a consistent power supply. Simulation and experimental results have verified the effectiveness of the proposed method, demonstrating its ability to mitigate voltage and current distortions during transitions. This ensures safer and more reliable operation of grid-connected inverters.

Although the validation of the proposed method demonstrates its potential for industrial application, further research is required to fully assess its wider applications and limitations. Furthermore, given the successful implementation of seamless transitions between the GFL and GFM control for a single grid-connected inverter, future research could focus on coordinating multiple grid-connected inverters within large-scale power systems. Ensuring effective collaboration among these inverters is crucial for enhancing the reliability and performance of power-electronic-based power systems in an increasingly renewable energy-dominated grid.

REFERENCES

[1] X. Gao, D. Zhou, A. Anvari-Moghaddam and F. Blaabjerg, "Seamless Transitions Between Grid-Following and Grid-Forming Control: A Novel Switching Method," in *Proc. 11th Int. Conf. Power Electron.* ECCE Asia, pp. 1154-1160, 2023.

[2] F. Blaabjerg, Y. Yang, D. Yang and X. Wang, "Distributed Power-Generation Systems and Protection," *Proceedings of the IEEE*, vol. 105, no. 7, pp. 1311-1331, July 2017.

[3] J. Rocabert, A. Luna, F. Blaabjerg, and P. Rodríguez, "Control of Power Converters in AC Microgrids," *IEEE Trans. Power Electron.*, vol. 27, no. 11, pp. 4734-4749, Nov. 2012.

[4] D. Dong, B. Wen, D. Boroyevich, P. Mattavelli and Y. Xue, "Analysis of Phase-Locked Loop Low-Frequency Stability in Three-Phase Grid-Connected Power Converters Considering Impedance Interactions," *IEEE Trans. Ind. Electron.*, vol. 62, no. 1, pp. 310-321, Jan. 2015.

[5] Q. Zhong and G. Weiss, "Synchronverters: Inverters That Mimic Synchronous Generators," *IEEE Trans. Ind. Electron.*, vol. 58, no. 4, pp. 1259-1267, April 2011.

[6] X. Gao, D. Zhou, A. Anvari-Moghaddam and F. Blaabjerg, "Stability Analysis of Grid-Following and Grid-Forming Converters Based on State-Space Model," *IEEE Trans. Ind. Appl.*, vol. 60, no. 3, pp. 4910-4920, May-June 2024.

[7] Y. Li, Y. Gu, and T. C. Green, "Revisiting Grid-Forming and Grid-Following Inverters: A Duality Theory," *IEEE Trans. Power Syst.*, vol. 37, no. 6, pp. 4541-4554, Nov. 2022.

[8] X. Wang, M. G. Taul, H. Wu, Y. Liao, F. Blaabjerg, and L. Harnefors, "Grid-Synchronization Stability of Converter-Based Resources—An Overview," *IEEE Open J. Ind. Appl.*, vol. 1, pp. 115-134, 2020.

[9] A. Singhal, T. L. Vu and W. Du, "Consensus Control for Coordinating Grid-Forming and Grid-Following Inverters in Microgrids," *IEEE Trans. Smart Grid*, vol. 13, no. 5, pp. 4123-4133, Sept. 2022.

[10] C. Yang, L. Huang, H. Xin and P. Ju, "Placing Grid-Forming Converters to Enhance Small Signal Stability of PLL-Integrated Power Systems," *IEEE Trans. Power Syst.*, vol. 36, no. 4, pp. 3563-3573, July 2021.

[11] M. Ganjian-Aboukheili, M. Shahabi, Q. Shafiee, and J. M. Guerrero, "Seamless Transition of Microgrids Operation From Grid-Connected to Islanded Mode," *IEEE Trans. Smart Grid*, vol. 11, no. 3, pp. 2106-2114, May 2020.

[12] D. S. Ochs, B. Mirafzal, and P. Sotoodeh, "A Method of Seamless Transitions Between Grid-Tied and Stand-Alone Modes of Operation for Utility-Interactive Three-Phase Inverters," *IEEE Trans. Ind. Appl.*, vol. 50, no. 3, pp. 1934-1941, May-June 2014.

[13] F. Sadeque, D. Sharma, and B. Mirafzal, "Seamless Grid-Following to Grid-Forming Transition of Inverters Supplying a Microgrid," in *Proc. Appl. Power Electron. Conf. Expo*., pp. 594-599, 2023.

[14] K. Lo and Y. Chen, "Design of a Seamless Grid-Connected Inverter for Microgrid Applications," *IEEE Trans. Smart Grid*, vol. 11, no. 1, pp. 194-202, Jan. 2020.

[15] H. Qing, C. Zhang, J. Xu, S. Zeng and X. Guo, "A Nonlinear Multimode Controller for Seamless off-Grid of Energy Storage Inverter Under Unintentional Islanding," *IEEE Trans. Ind. Electron.*, vol. 70, no. 12, pp. 12354-12364, Dec. 2023.

[16] S. Chakraborty, S. Patel, G. Saraswat, A. Maqsood and M. V. Salapaka, "Seamless Transition of Critical Infrastructures Using Droop-Controlled Grid-Forming Inverters," *IEEE Trans. Ind. Electron.*, vol. 71, no. 2, pp. 1535-1546, Feb. 2024.

[17] J. Wang, S. Ganguly and B. Kroposki, "Study of Seamless Microgrid Transition Operation Using Grid-Forming Inverters," *in Proc. 49th Ann. Conf. IEEE Ind. Electron. Soc.* IECON, pp. 1-6, 2023.

[18] M. Kwon, S. Park, C. Oh, J. Lee, and S. Choi, "Unified Control Scheme of Grid-Connected Inverters for Autonomous and Smooth Transfer to Stand-Alone Mode," *IEEE Trans. Power Electron.*, vol. 37, no. 1, pp. 416-425, Jan. 2022.

[19] R. Teodorescu and F. Blaabjerg, "Flexible control of small wind turbines with grid failure detection operating in stand-alone and grid-connected mode," *IEEE Trans. Power Electron.*, vol. 19, no. 5, pp. 1323-1332, Sept. 2004.

[20] C. Zhang, J. Zhang and C. Wang, "Research on Seamless Switching Between Islanded and Grid-Connected Operations of Photovoltaic Inverters Based on Model Prediction," *in Proc. 49th Ann. Conf. IEEE Ind. Electron. Soc.* IECON, pp. 1-6, 2023.

[21] F. Sadeque, M. Gursoy and B. Mirafzal, "Grid-Forming Inverters in a Microgrid: Maintaining Power During an Outage and Restoring Connection to the Utility Grid Without Communication," *IEEE Trans. Ind. Electron.*, vol. 71, no. 10, pp. 11796-11805, Oct. 2024.

[22] F. Sadeque, M. Gursoy, D. Sharma and B. Mirafzal, "Autonomous Control of Inverters in Microgrid," *IEEE Trans. Ind. Appl.*, vol. 60, no. 3, pp. 4313-4323, May-June 2024.

[23] A. B. Piardi, E. L. Geraldi, A. P. Grilo, R. Reginatto, and R. A. Ramos, "A Control Structure for Smooth Transfer From Grid-Connected to Islanded Operation of Distributed Synchronous Generators," *IEEE Trans. Power Del.*, vol. 35, no. 2, pp. 929-936, April 2020.

[24] H. M. A. Antunes, S. M. Silva, D. I. Brandao, A. A. P. Machado, and B. de Jesus Cardoso Filho, "A new multifunctional converter based on a series compensator applied to AC microgrids," *Int. J. Elect. Power Energy Syst.*, vol. 102, pp. 160–170, Nov. 2018.

[25] L. Yang, Y. Chen, A. Luo, Z. Chen, L. Zhou, X. Zhou, W. Wu, W. Tan, and J. M. Guerrero, "Effect of phase-locked loop on small-signal perturbation modeling and stability analysis for three-phase lcl-type inverter connected to weak grid," *IET Renew. Power Gen.*, vol. 13, no. 1, pp. 86–93, 2019.

[26] X. Li and H. Lin, "A Design Method of Phase-Locked Loop for Grid-Connected Converters Considering the Influence of Current Loops in Weak Grid," *IEEE J. Emerg. Sel. Top. Power Electron.*, vol. 8, no. 3, pp. 2420-2429, Sept. 2020.

[27] L. Huang, C. Wu, D. Zhou and F. Blaabjerg, "Impact of Grid Strength and Impedance Characteristics on the Maximum Power Transfer Capability of Grid-Connected Inverters," *Appl. Sci.*, vol. 11, no. 9, pp. 1-15, May 2021.

[28] R. H. Lasseter, Z. Chen, and D. Pattabiraman, "Grid-Forming Inverters: A Critical Asset for the Power Grid," *IEEE J. Emerg. Sel. Top. Power Electron.*, vol. 8, no. 2, pp. 925-935, Jun. 2020.

[29] D. Pattabiraman, R. H. Lasseter, and T. M. Jahns, "Comparison of Grid

Following and Grid Forming Control for a High Inverter Penetration Power System," in *Proc. of PESGM 2018*, pp. 1-5, 2018.
[30] B. Wen, D. Boroyevich, R. Burgos, P. Mattavelli, and Z. Shen, "Analysis of D-Q Small-Signal Impedance of Grid-Tied Inverters," *IEEE Trans. Power Electron.*, vol. 31, no. 1, pp. 675-687, Jan. 2016.
[31] G. Wu, H. Sun, X. Zhang, A. Egea-Àlvarez, B. Zhao, S. Xu, S. Wang, and X. Zhou, "Parameter design oriented analysis of the current control stability of the weak-grid-tied VSC," *IEEE Trans. Power Del.*, vol. 36, no. 3, pp. 1458-1470, 2020.
[32] X. Gao, D. Zhou, A. Anvari-Moghaddam and F. Blaabjerg, "A Comparative Study of Grid-Following and Grid-Forming Control Schemes in Power Electronic-Based Power Systems," *Power Electronics and Drives*, vol. 8, no. 1, pp. 1-20, Jan. 2023.
[33] M. Chen, D. Zhou, and F. Blaabjerg, "Voltage Control Impact on Performance of Virtual Synchronous Generator," in *Proc. 10th Int. Conf. Power Electron.* ECCE Asia, pp. 1981-1986, 2021.
[34] Y. Peng, D. Vrancic and R. Hanus, "Anti-windup, bumpless, and conditioned transfer techniques for PID controllers," *IEEE Control Syst.*, vol. 16, no. 4, pp. 48-57, Aug. 1996.
[35] Inaugural Research Agenda, "Global power system transformation (G-PST) consortium," Denver, CO, USA, 2021. [Online]. Available: https://globalpst.org/wp-content/uploads/042921G-PST-Research-Agenda-Mast er-Document-FINAL_updated.pdf.
[36] W. Dong, H. Xin, D. Wu, and L. Huang, "Small signal stability analysis of multi-infeed power electronic systems based on grid strength assessment," *IEEE Trans. Power Syst.*, vol. 34, no. 2, pp. 1393–1403, Mar. 2019.
[37] Y. Liu, X. Lai, H. Xin, J. Zhu, L. Huang and S. Xia, "Generalized Short-Circuit Ratio Based Distributed Real-Time Stability Assessment of Renewable Power Systems," *IEEE Trans. Power Syst.*, vol. 38, no. 6, pp. 5953-5956, Nov. 2023.
[38] D. Zhou, and F. Blaabjerg, "Bandwidth oriented proportional-integral controller design for back-to-back power converters in DFIG wind turbine system," *IET Renewable Power Generation*, vol. 11, no. 7, pp. 941-951, 2017.

Xian Gao (Member, IEEE) received the B.S. degree from Nanjing University of Information Science and Technology, Nanjing, China, in 2017, the M.S. degree from University of Chinese Academy of Sciences, Beijing, China, in 2020, and the Ph.D. degree from Aalborg University, Aalborg, Denmark, in 2024, all in electrical engineering. She was a visiting scholar with Imperial College, London, United Kingdom, in 2023. Since 2024, she has been with the College of Information Science and Technology & College of Artificial Intelligence, Nanjing Forestry University, Nanjing, China, where she is currently a lecturer. Her current research interests include stability and control of power-electronics-based power systems. She was a recipient of Best Paper Award at IEEE ICPE 2023-ECCE Asia.

Dao Zhou (S'12, M'15, SM'18) received the B.S. from Beijing Jiaotong University, Beijing, China, in 2007, the M. S. from Zhejiang University, Hangzhou, China, in 2010, and the Ph.D. from Aalborg University, Aalborg, Denmark, in 2014, all in electrical engineering.
Since 2014, he has been with Department of Energy, Aalborg University, where currently he is an Associate Professor. His research interests include modeling, control, and reliability of power electronics in renewable energy applications. He serves as an Associate Editor for IEEE Trans. on Industry Applications. He received a few IEEE prize paper awards.

Amjad Anvari-Moghaddam (S'10 - M'14 -SM'17) is an Associate Professor and Leader of Intelligent Energy Systems and Flexible Markets (iGRIDS) Research Group at the Department of Energy (AAU Energy), Aalborg University where he is also acting as the Vice-Leader of Power Electronic Control, Reliability and System Optimization (PESYS) and the coordinator of Integrated Energy Systems Laboratory (IES-Lab). His research interests include planning, control and operation management of microgrids, renewable/hybrid power systems and integrated energy systems with appropriate market mechanisms. He has (co)authored more than 300 technical articles, 8 books and 19 book chapters in the field. Dr. Anvari-Moghaddam is the Editor-in-Chief of Academia Green Energy journal and serves as the Associate Editor of several leading journals such as the IEEE TRANSACTIONS ON POWER SYSTEMS, IEEE Systems Journal, IEEE Open Access Journal of Power and Energy, and IEEE Power Engineering Letters. He is the Chair of IEEE Denmark, Member of IEC SC/8B- Working Group (WG3 & WG6) as well as Technical Committee Member of several IEEE PES/IES/PELS and CIGRE WGs. He was the recipient of 2020 and 2023 DUO–India and SPARC Fellowship Awards, DANIDA Research Fellowship grant from the Ministry of Foreign Affairs of Denmark in 2018 and 2021, IEEE-CS Outstanding Leadership Award 2018 (Halifax, Nova Scotia, Canada), and the 2017 IEEE-CS Outstanding Service Award (Exeter-UK).

Frede Blaabjerg (S'86–M'88–SM'97–F'03) was with ABB-Scandia, Randers, Denmark, from 1987 to 1988. From 1988 to 1992, he got the PhD degree in Electrical Engineering at Aalborg University in 1995. He became an Assistant Professor in 1992, an Associate Professor in 1996, and a Full Professor of power electronics and drives in 1998 at AAU Energy. From 2017 he became a Villum Investigator. He is honoris causa at University Politehnica Timisoara (UPT), Romania in 2017 and Tallinn Technical University (TTU), Estonia in 2018.

His current research interests include power electronics and its applications such as in wind turbines, PV systems, reliability, Power-2-X, power quality and adjustable speed drives. He has published more than 600 journal papers in the fields of power electronics and its applications. He is the co-author of eight monographs and editor of fourteen books in power electronics and its applications eg. the series (4 volumes) Control of Power Electronic Converters and Systems published by Academic

Press/Elsevier.

He has received 38 IEEE Prize Paper Awards, the IEEE PELS Distinguished Service Award in 2009, the EPE-PEMC Council Award in 2010, the IEEE William E. Newell Power Electronics Award 2014, the Villum Kann Rasmussen Research Award 2014, the Global Energy Prize in 2019 and the 2020 IEEE Edison Medal. He was the Editor-in-Chief of the IEEE TRANSACTIONS ON POWER ELECTRONICS from 2006 to 2012. He has been Distinguished Lecturer for the IEEE Power Electronics Society from 2005 to 2007 and for the IEEE Industry Applications Society from 2010 to 2011 as well as 2017 to 2018. In 2019-2020 he served as a President of IEEE Power Electronics Society. He has been Vice-President of the Danish Academy of Technical Sciences.

He is nominated in 2014-2021 by Thomson Reuters to be between the most 250 cited researchers in Engineering in the world.